Local Structural Characterization for Electrochemical Insertion−Extraction of Lithium into CoO with X-ray Absorption Spectroscopy

Hyun Chul Choi, Sang Yun Lee, and Seung Bin Kim*

Department of Chemistry, Pohang University of Science and Technology, Hyojadong, Namgu, Pohang 790-784, Republic of Korea

Min Gyu Kim, Min Kyu Lee, Hyun Joon Shin, and Jae Sung Lee

Pohang Accelerator Laboratory and Department of Chemical Engineering, Pohang University of Science and Technology, Hyojadong, Namgu, Pohang 790-784, Republic of Korea

Received: March 1, 2002; In Final Form: June 17, 2002

Cobalt oxide is known to exhibit a large capacity as a negative electrode in lithium-ion batteries. Here, Co K-edge X-ray absorption spectroscopy (XAS) was used to investigate variations in the local structure during the first electrochemical cycle of the insertion−extraction of lithium into CoO. The XANES and EXAFS spectra in Li_yCoO (y: lithium content) varied markedly with the lithium content. The initial insertion of lithium leads to the reduction of Co^{2+} in the pristine CoO to the reduced metallic Co^0 state. The systematic variations observed in intensities of the peaks corresponding to the 1s → 3d and 1s → 4p transitions indicate that the mole ratio of Co to CoO increases gradually with the electrochemical insertion of lithium ions. Insertion of lithium causes the local structure around the Co atoms to become asymmetric. The systematic decrease in the magnitude of the Fourier transform (FT) with increasing amount of inserted lithium is closely related to an increase in static disorder due to the presence of two phases: Co^0 clusters and CoO. The small-sized Co particles evolve gradually with a well-separated distribution in the Li_2O matrix. In the successive extraction of lithium, the reduced Co particles return reversibly to the high-temperature cubic phase of CoO.

Introduction

The lithium-ion battery has the highest energy density among commercial rechargeable batteries. Commercial rechargeable lithium batteries use a transition metal oxide as the positive electrode and a carbonaceous material as the negative electrode.[1,2] The strong demand of the portable electronics market for power sources with the longest possible life has prompted the development of high energy density batteries. Progress in the development of such batteries has been linked to the availability of advanced electrode materials, and various electrode materials have been investigated for secondary lithium batteries.

The use of metal oxides as anodes in rechargeable lithium batteries has drawn great attention due to the high specific capacity of these materials. For example, Idota et al. have synthesized an amorphous tin oxide with 400−500 (Ah)/kg capacity and an average discharge voltage vs Li metal of about 0.4 V.[3] Leroux et al. examined the use of vanadium derivatives, $MV_2O_{6+\delta}$ (M = Mn, Co), as anodes in secondary lithium cells.[4] They found that $MnV_2O_{6.96}$ exhibited a capacity of 891 (mAh)/g and an average discharge voltage of 0.5 V. Denis et al. reported the performances of amorphous vanadates of general formula RVO_4 (R = In, Cr, Fe, Al, Y) synthesized via a low-temperature preparation method.[5] These compounds show a large capacity of 900 (mAh)/g during the first cycle. Although oxide anodes show a large capacity compared to carbon materials, oxides exhibit a large irreversible capacity or substantial loss of capacity.[6,7] Unfortunately, these electrochemical properties are unfavorable to the use of oxides as practical electrode materials.

* To whom correspondence should be addressed. Tel: +82-54-279-2106. Fax: +82-54-279-3399. E-mail: sbkim@postech.ac.kr.

Recently, the Tarascon group suggested the electrochemical insertion−extraction of Li^+ into the 3d-transition metal oxide MO (M = Co, Ni, Cu, etc.) according to the following reaction:[8,9]

$$MO + 2Li \rightleftharpoons Li_2O + M$$

These materials show a large capacity of 700 (mAh)/g up to 100 cycles, which is nearly twice the capacity generally found in carbon anodes. In addition, they suggested that a pseudo-amorphous metal oxide was formed during the first cycle. However, Obrovac et al. reported that the high-temperature cubic phase (rock salt structure) of CoO changed into zinc blende type CoO (low-temperature phase) by X-ray diffraction (XRD) characterizations during the discharging-charging process.[10]

The insertion−extraction reaction of Li^+ in the metal oxides induces local structural and electronic perturbations, which can affect the chemical and electrochemical properties of the material. Consequently, determination of the relationship between the local structure and the lithium content is very important to understanding of the electrochemical behavior of these electrode materials. However, XRD is limited to the study of bulk structural properties due to line broadening and it is difficult to determine the precise lattice parameters using this method.

In contrast to XRD, X-ray absorption spectroscopy (XAS) is known to provide valuable information about the local structure around an atom of interest. The absorption peak features in the X-ray absorption near edge structure (XANES) can be used to extract useful structural parameters such as the oxidation state

10.1021/jp0205968 CCC: $22.00
Published on Web 08/20/2002

of the chemical species, site symmetry, and covalent bond strength.[11−18] On the other hand, extended X-ray absorption fine structure (EXAFS) spectra can be used to obtain quantitative structural parameters such as interatomic distance, coordination number, and Debye−Waller factor.[19−23] EXAFS is a powerful technique for local structural analysis of short-range ordered compounds because it is very sensitive to the local atomic environment and does not depend on long-range order.

The objective of the present study was to elucidate the mechanism of the lithium reaction with CoO from the viewpoint of the local geometric and electronic structures. To achieve this objective, systems of formula Li_yCoO, where y is the lithium content, were studied during the first cycle using Co K-edge XAS. In addition, Co $L_{II,III}$-edge and oxygen K-edge XAS were used to investigate variations in the electronic structure upon insertion−extraction of Li^+ into CoO. We found that lithium insertion is accompanied by the formation of clusters of metallic Co which are reversibly oxidized to the high-temperature cubic phase of CoO after the first cycle.

Experimental Section

Electrochemical Experiments. Electrochemical behavior of cobalt oxide was investigated in organic electrolyte lithium cells. Slurries were prepared that consisted of 80 wt % cobalt oxide powder (Aldrich, 325 mesh), 10 wt % acetylene black, and 10 wt % polyvinylidene fluoride (PVDF) dissolved in *n*-methylpyrrolidinone. Electrodes were made by coating the slurry onto an aluminum foil substrate. Test cells were fabricated with these electrodes, metallic Li anodes, and polypropylene separators (Celgard 2400) in a glovebox filled with Ar gas. A 1.0 M solution of $LiPF_6$ in ethylene carbonate−diethyl carbonate (1:1 by volume) was used as the electrolyte. Cell performance was evaluated by galvanostatically discharging and charging the cell at a constant current density of 0.5 mA/cm^2 at room temperature with a WBCS 3000 battery tester system (Won A Tech Corp.). Electrochemical impedance spectroscopy measurements were carried out using an HS-3E Test cell (Hohsen three electrode cell, Hohsen Co.). The test cell was constructed using the composite electrode (CoO) as a working electrode and the lithium metal as counter and reference electrodes. The impedance experiments were carried out at different potentials on the Li_yCoO electrode. Data were collected in the frequency range from 0.01 Hz to 100 kHz with an ac voltage signal of ±5 mV with an IM6 analyzer (Zahner, Germany).

Co K-Edge XAS Measurements. Co K-edge X-ray absorption spectra were recorded using the BL3C1 beam line of the Pohang Light Source (PLS) with a ring current of 120−170 mA at 2.5 GeV. A Si(111) monochromator crystal was used with detuning to 85% in intensity to eliminate high-order harmonics. Data were collected in transmission mode using gas-filled ionization chambers (85% nitrogen, 15% argon) as detectors. Energy calibration was carried out for all measurements using Co foil placed in front of the third ion chamber, assigning the first inflection point to 7709 eV.

Co $L_{II,III}$-Edge and Oxygen K-Edge XAS Measurements. Co $L_{II,III}$-edge and oxygen K-edge XAS measurements of the Li_yCoO were performed on the U7 beamline at PLS. The U7 beamline, which consists of an undulator (length 4.3 m, period 7 cm) and a variable-included-angle plane-grating monochromator, provides highly brilliant and monochromatic linear-polarized soft X-rays suitable for high-resolution spectroscopy. The Co $L_{II,III}$-edge and O K-edge XAS data were taken in total electron yield mode, recording the sample current. The details pertaining to the design of the monochromator and resolution are given elsewhere.[24,25] The energy resolution at the Co 2p and O 1s absorption edges was set to approximately 0.2 eV. The Co $L_{II,III}$-edge and O K-edge energies were calibrated using data from the L-edges of pure Co and V metal foils, respectively. The experimental spectra were normalized by a reference signal from Au mesh with 90% transmission. The base pressure of the experimental chamber was in the 10^{-8} mbar range.

Co K-Edge EXAFS Data Analysis. The EXAFS data analysis was carried out using the standard procedure described elsewhere.[19,20] The measured absorption spectra below the pre-edge region were fitted to a straight line, and then the background contribution above the post-edge region, $\mu_0(E)$, was fitted to a high-order polynomial (cubic spline). The fitted polynomials were extrapolated over the entire energy region and subtracted from the total absorption spectra. The absorption spectra with the background subtracted were normalized for the above energy region, $\chi(E) = \{\mu(E) - \mu_0(E)\}/\mu_0(E)$.The normalized k^3-weighted EXAFS spectra, $k^3\chi(k)$, were Fourier transformed in the k range from 2.0 to 14.5 Å^{-1} to show the contribution of each bond pair to the Fourier transform (FT) peak. The experimental Fourier-filtered $k^3\chi(k)$ spectra were obtained from the inverse Fourier transformation with the hanning window function in the r space range of 1.0 and 6.0 Å. To determine the structural parameters for each bond pair, the curve fitting process was carried out by using the EXAFS formula:[19]

$$\chi(k) = \sum N_j S_i^2(k) F_j(k) \exp(-2\sigma_j^2 k^2) \exp(-2r_j/\lambda_j(k)) \frac{\sin(2kr_j + \Phi_{ij}(k))}{kr_j^2}$$

where k is the photoelectron wave vector, N_j is the coordination number, S_i^2 is the amplitude reduction factor, $F_j(k)$ is the effective curved-wave backscattering amplitude, σ_j^2 is the Debye−Waller factor, λ is the mean free path of the photoelectron, r_j is the interatomic distance, and Φ_{ij} is total phase shift.

Theoretical scattering paths were obtained from the crystallographic description of the known model. The theoretical EXAFS parameters such as phase shift, backscattering amplitude, and total central atom loss factor were calculated as a function of wavenumber for all possible scattering paths by FEFF 6.01 code.[15,17] To simplify the curve fitting process, the value of S_i^2 for the Co atom was fixed at 0.85. The coordination numbers (N) were also fixed to the crystallographic values because the N value is highly correlated with the Debye−Waller factor in the amplitude of EXAFS spectra. The experimental $k^3\chi(k)$ spectra were fitted with possible scattering paths, showing the substantial amplitude for the corresponding FT peak. In the fitting process for the EXAFS spectra, only two structural parameters (the interatomic distance and the Debye−Waller factor) were used as adjustable parameters.

Results and Discussion

Figure 1 shows the voltage vs the lithium content curves for the Li/Li_yCoO cell, measured at a current density of 0.5 mA/cm^2 in the voltage range 0.2−3.2 V. Li_yCoO reacts with three lithium atoms per formula unit, and upon the following charging process about the half of them were removed. The average discharge voltage of this material is about 0.68 V vs Li metal.

It is expected that the insertion−extraction reaction of Li^+ in the Li_yCoO electrode affects the chemical and electrochemical properties of the electrode. Figure 2 shows the Nyquist plots

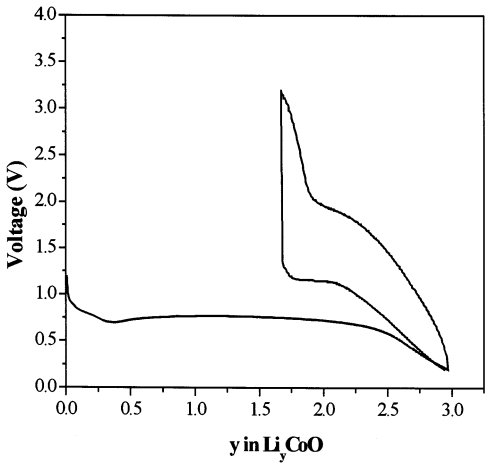

Figure 1. First cycle curve of Li_yCoO cell.

for the Li_yCoO electrode obtained at different potentials during the first cycle. Each plot consists of a depressed semicircle and a distorted Warburg tail or a capacitive loop. At higher frequencies the depressed semicircle can be attributed to the formation of passive films, whereas in the lower frequency range this feature is due to the charge transfer. The Warburg tail is assigned to solid-state diffusion of lithium ions into the bulk metal oxide. The straight line obtained at low frequency reflects the capacitive behavior resulting from the accumulation of the lithium in the bulk. ac impedance spectra decrease dramatically against the insertion of Li^+ during first discharging process. In contrast, the impedance value increases systematically with the extraction of Li^+ during the charging process. These results suggest that the overall electrical conductivity of the system changes with lithium content. To elucidate the local structure, XAS data were collected at various lithium contents during the first cycle.

Co K-Edge XANES Spectroscopy. Normalized Co K-edge XANES spectra from the Li_yCoO system in the first discharging process are shown in Figure 3. The pristine CoO that has a rock salt structure shows a weak absorption peak A at ~7710 eV due to the transition of 1s electrons to the unoccupied 3d−e_g orbital of the Co^{2+} ($t_{2g}^6e_g^1$) ion.[10,25−27] Although the 1s → 3d transition is electric dipole-forbidden in an ideal octahedral symmetry, the appearance of the weak absorption peak is due to pure electric quadrupole coupling and the noncentrosymmetric environment of the slightly distorted CoO_6 octahedral site. Peak B corresponding to the pristine CoO in Figure 3 is due to the electric dipole-allowed transition of a 1s core electron to an unoccupied 4p bound state with T_{1u} symmetry. Peak B corresponds to final state of $1s^1c3d^74p^1$, where *c* is a 1s core hole.[25,26]

As shown in Figure 3, the XANES spectra for electrochemical insertion of Li^+ change significantly with the *y* value. As the *y* value increases, the intensity of peaks A increases and the intensity of peaks B decreases monotonically. Similar to the behavior of peaks A, the main spectral features of peaks B show no noticeable variation for electrochemical insertion of Li^+ from the pristine CoO to 0.78 mol. The spectral features of the pristine CoO change abruptly when the insertion of Li^+ reaches 1.32 mol. The main features observed at higher values of the insertion of Li^+ show a greater resemblance to the feature of Co foil. This indicates that the electrochemical insertion of Li^+ leads to the reduced Co^0 state and, consequently, the gradual formation of Co clusters. However, even at the highest insertion of Li^+ ($y = 3.07$) its spectral feature is not exactly that of the reference spectrum of Co foil. This difference can be attributed to the long-range disorder in the Li_yCoO system caused by the division of Co into small clusters. Tarascon et al. have reported that the full insertion of Li^+ gives rise to the formation of metallic Co nanoparticles dispersed in the Li_2O matrix.[8] As the particle size decreases, the surface-to-volume ratio increases with a consequent increase in the fraction of Co atoms in distorted environments at surfaces. In the present study, therefore, the difference between the spectra of the fully lithiated Li_yCoO and the pure reference Co foil can be attributed to the structural difference between the pure Co in the reference foil and the Co in the nanoscale clusters in the Li_2O phase, the spectral feature of which is modified by the surface effect between the Co cluster and the Li_2O phase.

As mentioned above, the pre-edge peak intensity of the 1s → 3d electric quadrupole transition depends on the pure 3d character of the corresponding bound state under ideal octahedral symmetry. In the noncentrosymmetric environment, however, the distortion of the local structure around the Co atom gives rise to d−p mixing, which changes the relative 3d and 4p character and, therefore, the peak intensity. In the orbital mixing, the 1s → 3d quadrupole transition obtains the electric dipole coupling by the partial possession of p character. The loss of p character in the 1s → 4p electric dipole transition leads to the decrease observed in the intensities of peaks B. From the systematic variations of the peak intensity, it is found out that insertions of Li^+ equal to or higher than 1.32 mol in this study lead to distortion in the local structure around the Co atoms, and Co clusters begin to gradually evolve in the CoO phase.

Because the peak features are very sensitive to the local environment around each central cobalt ion, the structural and electronic variations associated with the change in lithium content can be probed by consideration of the position and intensity of the peaks in the XANES spectra. The mole ratios of Co to CoO were obtained from experimental XANES spectra of Li_yCoO by a simulation of the linear combination of reference spectra of Co foil and CoO. Figure 4 illustrates the relationship between the *y* value and the Co/CoO mole ratio. The peak intensity ratios change systematically with the lithium content. The linear relationship indicates that the mole ratio of Co to CoO within Li_yCoO increases with the *y* value. The spectral feature denoted as peak A in the insertion of Li^+ can, therefore, be described as being composed of two 1s → 3d quadrupole transitions: one for Co^0 and the other from Co^{2+}. The increase of the peak intensity ratio with the lithium content indicates the gradual evolution of Co^0 as the electrochemical insertion proceeds. However, the mole ratio of Co^0 to Co^{2+} ion could not be determined quantitatively from the pre-edge feature because the peaks could not be separated at the energy resolution ($\Delta E/E$) used for the measurements ($\sim 2.0 \times 10^{-4}$ eV). Only a systematic variation of the intensity of peak A was observed, which showed the increase of the mole ratio of Co to CoO with the insertion of Li^+.

Co K-edge XAS revealed that the insertion of Li^+ equal to or higher than 1.32 mol in this study led to a variation in the local structure around cobalt ions. The results described above prompt two important questions. First, where can we find the lithium inserted up to 0.78 mol in the pristine structure? Second, how do we account for the oxygen behavior, which cannot be explained by Co K-edge XAS? To address these questions, the Li_yCoO system was studied during the first cycle using the Co $L_{II,III}$-edge and oxygen K-edge XAS technique.

This technique is very sensitive to surface conditions and involves a probing depth of the X-ray absorption of approximately 50 Å.[28] Furthermore, this method provides site- and symmetry-selected information on the unoccupied electronic

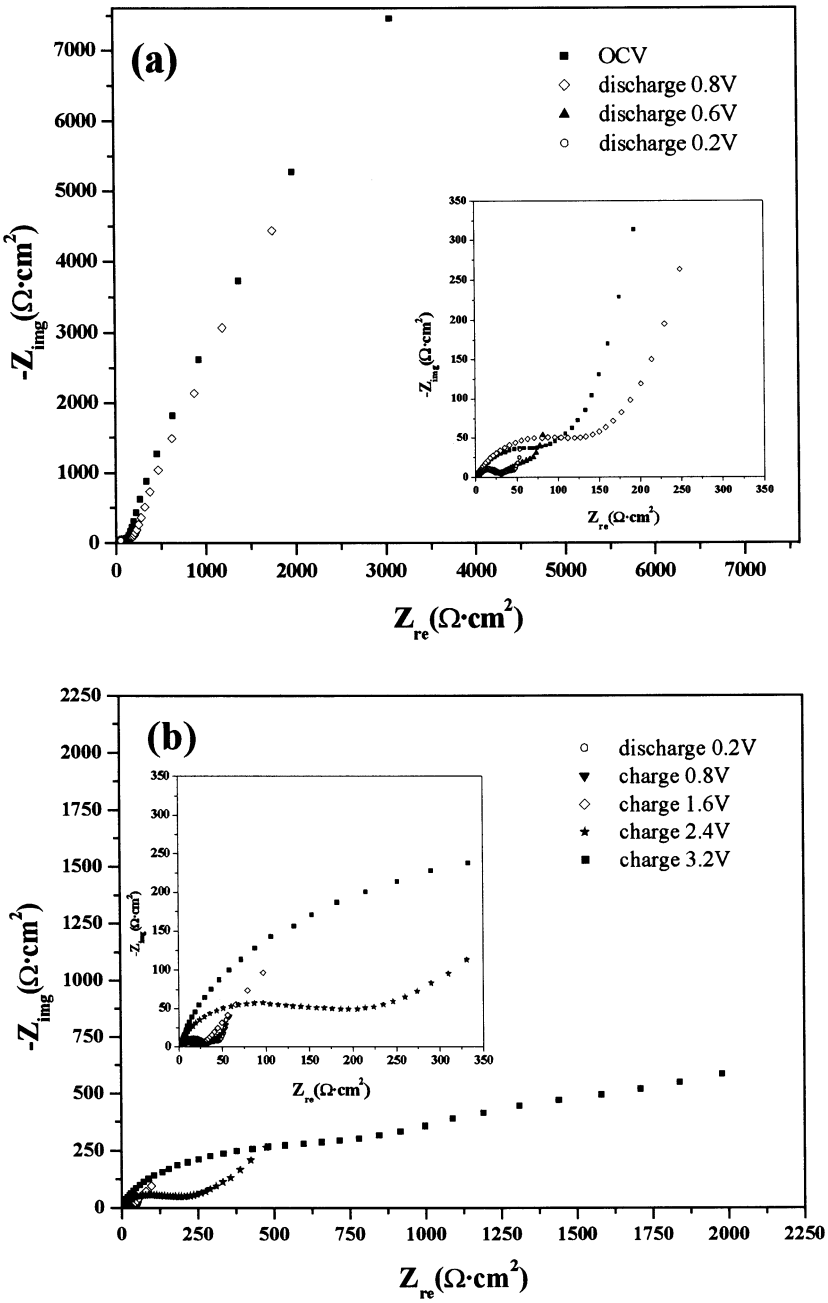

Figure 2. Nyquist plots of the Li_yCoO electrode obtained at (a) the discharging and (b) the charging process.

states.[29−31] The electric dipole-allowed 1s → 2p transition of oxygen K-edge XAS provides a direct probe of the oxygen charge state and Co−O bonding interaction because the 2p orbitals of the oxygen ligand are involved in a bonding configuration with the cobalt ion under octahedral symmetry. The characteristic pre-edge features correspond to the electronic transition from the oxygen 1s core electron to the unoccupied molecular level by the hybridization of the Co 3d orbital with the oxygen 2p orbital. The pre-edge peak position and intensity give important structural information about the chemical bonding between oxygen and Co atoms. In addition, direct information about the unoccupied molecular levels can be obtained from the intense absorption peaks of Co $L_{II,III}$-edge XAS, which represent the main 2p → 3d transition.

Figure 5 shows the oxygen K-edge XAS spectra of the Li_y-CoO system for the first cycle. The oxygen K-edge XAS of the pristine CoO shows the main peak at ∼529 eV due to the oxygen 1s electron to the hole state transition in the oxygen 2p level. The broad higher absorption peaks above 533 eV can be assigned to the transitions to hybridized states of oxygen 2p and Co 4sp orbitals.[25,28] In comparison to the pristine material, the oxygen K-edge XAS spectra change dramatically when the insertion of Li^+ reaches 0.96 mol. On further insertion of Li^+, the main spectral features vary only a small amount. A recent study of the electrochemical reaction of lithium with CoO suggests that the Li_2O is produced with the insertion of Li^+ during the first discharge process.[8,10] These studies also suggest that the cobalt nanoparticle and Li_2O matrix are surrounded by a solid electrolyte interface caused by the electrolyte decomposition reaction.[8,10] As shown in Figure 5, the spectral features of the Li_yCoO system are different from that of the reference spectrum of Li_2O and vary only a small amount during the electrochemical insertion−extraction reaction of Li^+. This indicates that when the insertion of Li^+ reaches 0.78 mol (see Figure 3), a great portion of the inserted lithium is consumed on the surface of CoO to form the solid electrolyte interface.

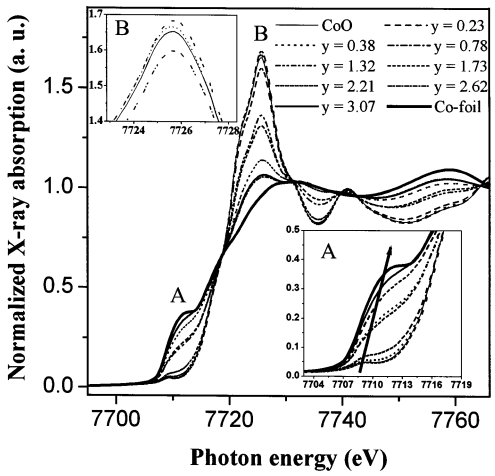

Figure 3. Normalized Co K-edge XANES spectra for the electrochemically lithium-ion inserted Li_yCoO system in the discharging process. The lithium content (y in Li_yCoO) is indicated in the figure.

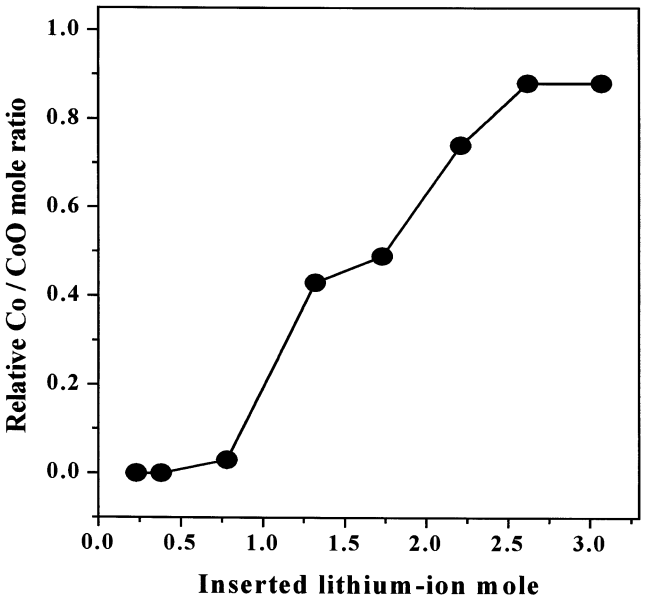

Figure 4. Mole ratio of Co to CoO vs the lithium content plot obtained from experimental XANES spectra of Li_yCoO by a simulation of the linear combination of reference spectra of Co foil and CoO.

As a result, no variation is observed in the main features of the Co K-edge XAS spectra, but the oxygen K-edge XAS spectra change significantly compared with the pristine material when the insertion of Li^+ reaches 0.96 mol.

Figure 6 shows the Co $L_{II,III}$-edge XAS spectra for the discharging process. The Co $L_{II,III}$-edge XAS of pristine CoO shows main peaks at ~776.6, ~777.6, and ~779 eV, and a weak shoulder peak at 793 eV, respectively, due to Co 2p−3d electrostatic interaction and crystal field effect of octahedral symmetry.[25] Upon the insertion of lithium, a clear change is observed in the intensity of the spectra compared with the pristine material. As the y value increases, the intense features of the pristine CoO become weaker dramatically. The intensity variations in the spectra suggest that the Co atoms are surrounded by a layer of passive film, the thickness and nature of which varies upon the insertion of lithium. Unfortunately, soft X-ray measurement is affected by surface properties such as thickness, composition, and roughness; hence, the behavior of the oxygen ion could not be observed from the Co $L_{II,III}$-edge and oxygen K-edge XAS.

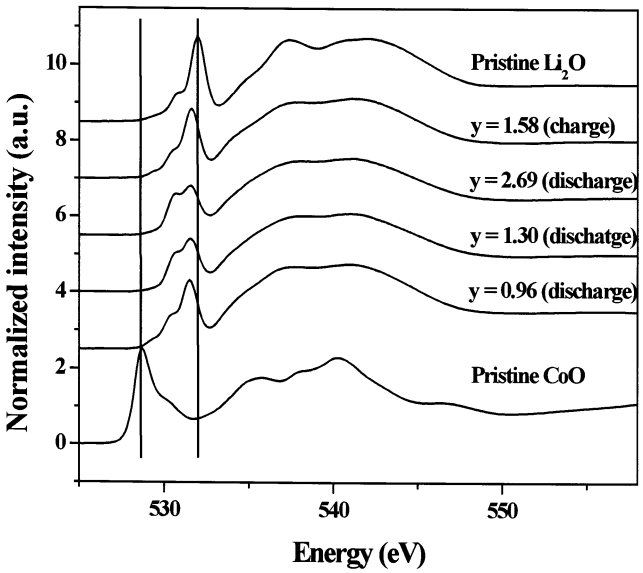

Figure 5. Normalized oxygen K-edge XAS spectra for the electrochemical lithium reaction.

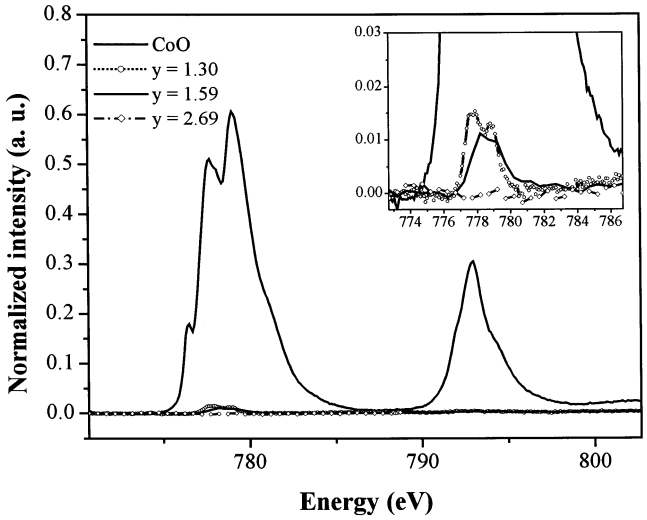

Figure 6. Normalized Co $L_{II,III}$-edge XAS spectra for the electrochemically lithium-ion inserted Li_yCoO system in the discharging process.

Figure 7 shows the XANES spectra for the electrochemical extraction of Li^+ in the charging process. The peak features approach those of CoO as more lithium is extracted from the Li_yCoO system. The spectrum of Li_yCoO ($y = 1.51$) obtained during the 3.2 V charging step shows the same spectral feature as the CoO spectrum, indicating that the electrochemical insertion−extraction process is reversible for the first cycle and the reduced Co^0 state returns to the Co^{2+} state. According to a recent in situ XRD study of the high-temperature phase of CoO in the discharging−charging process, the first insertion−extraction of Li^+ leads to the formation of zinc blende type CoO (low-temperature phase).[10] The reduced Co^0 in the discharging process is subsequently oxidized to Co^{2+}, which is then ion-exchanged with Li^+ from the Li_2O phase. It was suggested that the cubic CoO undergoes a phase transition to zinc blende type, because of the structural similarity of the zinc blende structure to Li_2O. In the XANES spectra, however, the first electrochemical process leads to reversible return to the high-temperature cubic phase. If the cubic phase changed to the zinc blende type, the peak features, especially the pre-edge peak A, would be very different from those of the high-temperature cubic phase of CoO because the Co atom in the

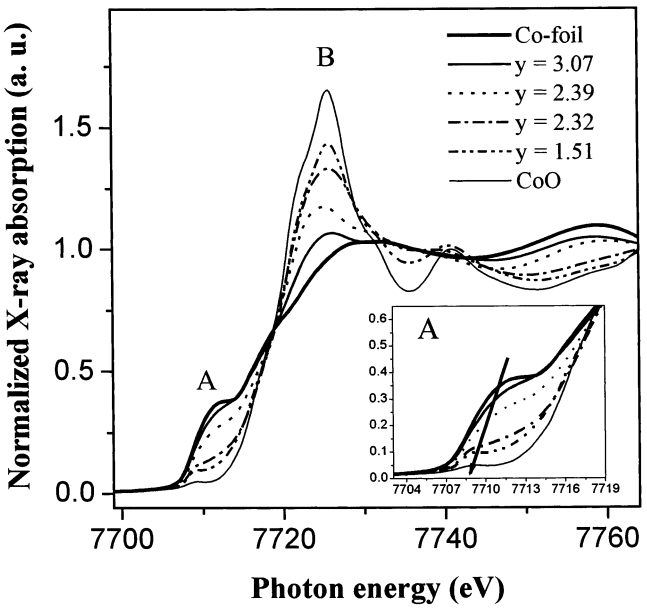

Figure 7. Normalized Co K-edge XANES spectra for the electrochemically lithium-ion extracted Li_yCoO system in the charging process.

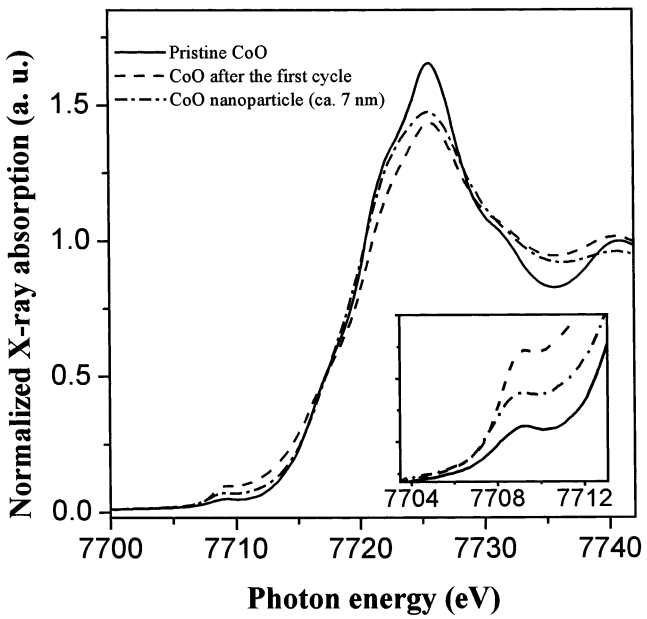

Figure 8. Comparison of the spectra from the pristine CoO, CoO after the first cycle, and CoO nanoparticle (ca. 7 nm). Here, the CoO nanoparticle was prepared as described earlier by Park et al.[32] The nanosized Co powder (approximately 7 nm) was oxidized in the atmosphere for XAS measurement.

zinc blende structure occupies a tetrahedral site. The lower symmetry of the tetrahedral site would give rise to substantial spectral variation.

The XANES spectrum of the nanoparticle CoO (ca. 7 nm) is presented in Figure 8, along with the spectrum of CoO after the first cycle. In comparison to the pristine material, the XANES spectrum of CoO after the first cycle shows a more intense peak A and a less intense peak B. With disregard to Li_2O matrix, this difference can be attributed to the particle size effect such as decreased coordination number and the 3d−4p orbital mixing caused by the surface distortion. The present results, therefore, show a return to similar peak features after the first electrochemical process, indicating that the high-temperature cubic phase of CoO returns.

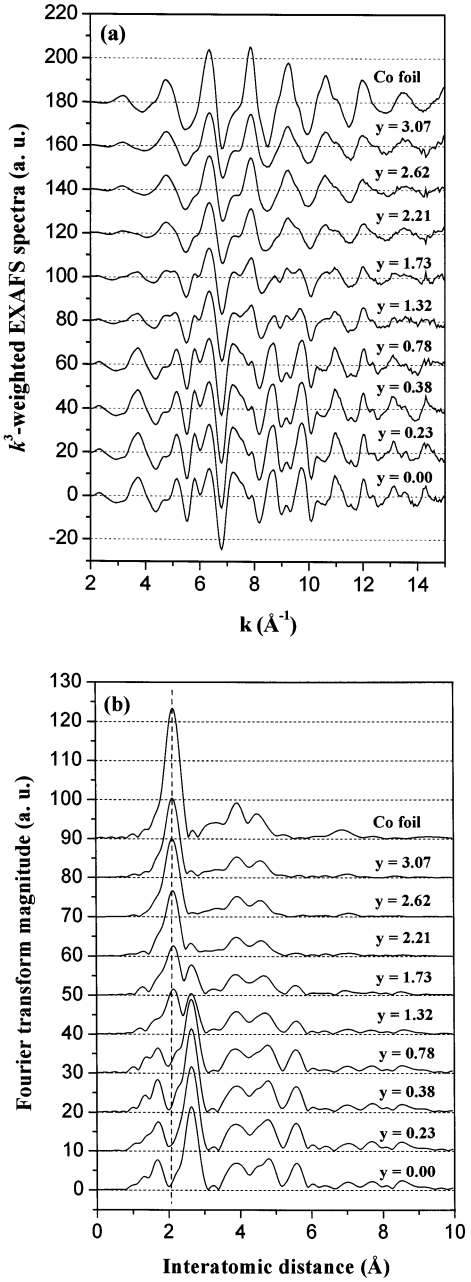

Figure 9. (a) Co K-edge $k^3\chi(k)$ spectra and (b) their Fourier transforms (FTs) for the electrochemically lithium-ion inserted Li_yCoO system.

Co K-Edge EXAFS Spectroscopy. Parts a and b of Figure 9 show k^3-weighted $\chi(k)$ spectra and their Fourier transforms (FTs) for the Li_yCoO system, respectively. The principal peaks in the FT between 1.0 and 6.0 Å in Figure 9b provide important structural information because the FT peaks are closely associated with the site symmetry around the central Co atom. For the pristine CoO, the FT peak at ∼1.7 Å corresponds to six-coordinated oxygen nearest neighbors around the Co atom, whereas the peak at ∼2.6 Å is assigned to the contribution of 12-coordinated Co atoms in the next edge-shared octahedral site.[33,34] The results show that the main contribution to the FT magnitude of ∼3.9 Å is from the double scattering path of Co → O → Co in the corner-shared octahedra. The magnitudes of FT at ∼4.8 and ∼5.6 Å correspond to the single scattering path of Co → Co and the focused double scattering of Co → Co → Co in the edge-shared octahedral layer, respectively.[35]

As shown in Figure 9b, the electrochemical insertion of Li^+ up to 0.78 mol leads to a decrease in the magnitude of the FT

peaks of pure CoO without the overall spectral shape changed. Generally, local structural parameters such as the particle size and the coordination number are linearly dependent upon the FT peak intensity in the EXAFS. If the insertion of Li^+ up to 0.78 mol into CoO induces the local structural distortion, which can affect the scattering path, the FT peak intensities at 3.9, 4.8, and 5.6 Å should decrease dramatically. However, the FT peak intensities at 3.9, 4.8, and 5.6 Å decrease with respect to those of the CoO and their spectral features remain as described above, which indicates that the high-temperature cubic phase is maintained despite the insertion of Li^+. This observation indicates that the insertion of Li^+ leads to a decrease in the size of the particles containing CoO during the insertion of Li^+.

As shown in Figure 9b, for insertions of Li^+ equal to or above 1.32 mol, the major change in the FT is the evolution of a new peak at ~2.1 Å. This new peak is characteristic of the reduced Co^0 phase and corresponds to six-coordinated Co atoms as the nearest neighbors around a Co atom.[33,34] The emergence of this peak, therefore, results from the gradual formation of metallic Co^0 phase in the Li_yCoO system. For Li^+ insertions equal to or above 2.62 mol in Figure 9b, the FT peak corresponding to edge-shared Co → Co single scattering in CoO at ~2.5 Å almost disappears. Further insertion of Li^+ up to 3.07 mol has no effect on the local structure of the Co^0 phase; thus, the formation of the Co^0 phase is terminated at the lithium content of about 2.62 mol in this study. Hence, these observations are in good agreement with a recent report that the electrochemical reaction is $2Li^+ + CoO + 2e^- \rightarrow Li_2O + Co$.[8]

To obtain the quantitative information of the cobalt site in the lithiated CoO, the experimental EXAFS spectra were simulated by FEFF code in the single scattering region. Parts a and b of Figure 10 show the experimental Fourier-filtered $k^3\chi(k)$ spectra and Fourier transforms (the solid line) and best-fit $k^3\chi(k)$ spectra and Fourier transforms (the dot line) for the $Li_{1.73}CoO$, respectively. In the theoretical scattering calculations, the contributions of the lithium atom to the EXAFS signal were not considered because the backscattering amplitude of the photoelectron for the lithium atom is very weak. The local structural parameters of $Li_{1.73}CoO$ obtained from EXAFS refinement are listed in Table 1 with the pristine CoO and Co foil together. The most relevant data from this table in connection with the objectives of this study are coordination number and Debye−Waller factor. The coordination numbers of the CoO and Co phases in $Li_{1.73}CoO$ are approximately half (Co−O in CoO), a third (Co−Co in CoO), and half (Co−Co in Co foil) of the bulk values, respectively. Because the surface-to-volume ratio and the number of distorted sites at the surface increase as the particle size decreases, the number of neighboring atoms corresponding to each bonding pair decreases linearly. These results indicate that the two phases are distributed independently with a smaller particle size than the bulk CoO and Co foil.

In the present system, the insertion of Li^+ into bulk CoO gives rise to a nanoscale Co^0 phase. The Debye−Waller factors (σ) of the $Li_{1.73}CoO$ (σ is a measurement of the disorder degree around the central Co) are higher than in the reference materials. Also, the FT peak intensities of the Co^0 phase in the $Li_{2.62}CoO$ and $Li_{3.07}CoO$ are about two-thirds of the corresponding intensities for Co^0 foil (see Figure 9b). The magnitude of the FT peak of a bond pair is inversely related to the Debye−Waller factor corresponding to the mean square relative displacement (MSRD) of the interatomic distance due to static disorder and thermal vibrational disorder. In the present system, the systematic decrease in the FT magnitudes is primarily due to an increase in static disorder rather than a thermal vibrational effect. These results indicate that the insertion of Li^+ into CoO induces local structural distortion corresponding to the relative amount of Co^0 and CoO in the Li_yCoO system, which can affect the FT magnitude in the EXAFS.

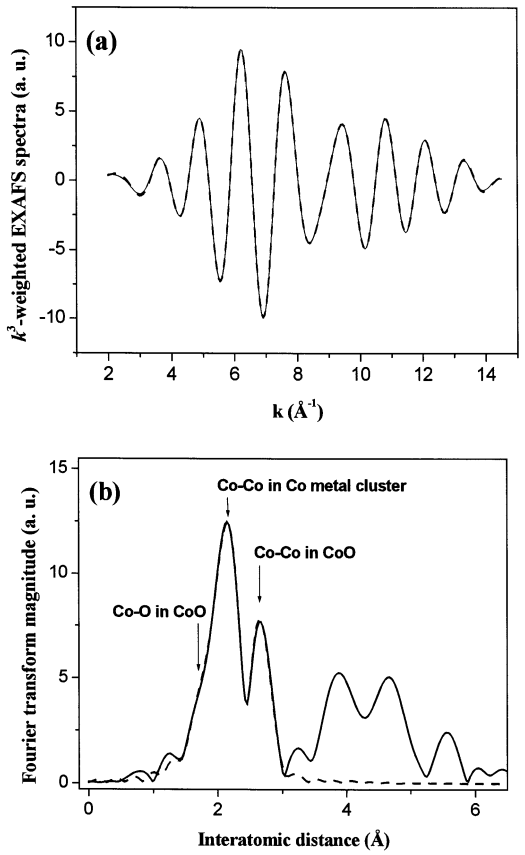

Figure 10. (a) Experimental Fourier-filtered $k^3\chi(k)$ spectra and Fourier transforms (solid line) and (b) best-fitted $k^3\chi(k)$ spectra and Fourier transforms (dashed line) for $Li_{1.73}CoO$, respectively.

TABLE 1: Local Structural Parameters of Co K-Edge EXAFS Refinement for $Li_{1.73}CoO$[a]

sample	shell	ΔE, eV	R (Å)	N	σ^2 ($\times 10^{-3}$ Å^2)
Pristine CoO	Co−O	−1.3	2.126	6.0	6.73
	Co−Co	3.1	3.016	12.0	7.43
$Li_{1.73}CoO$	Co−O	−2.8	2.114	2.7	7.01
	Co−Co	−2.6	2.509	6.1	6.22
	Co−Co	−2.0	3.009	3.6	9.21
Co foil	Co−Co	−0.5	2.501	12.0	5.56

[a] Energy variation (ΔE), bond length (R), coordination number (N), and variation in Debye−Waller factor (σ^2) obtained from FEFF 6.01 code. In the curve fitting process, the goodness of fit by $\{\Sigma(k^3\chi_{data} - k^3\chi_{model})^2\}/\Sigma(k^3\chi_{data})^2$ has been estimated within the allowed error range. The estimated errors are within ±0.02 Å for the interatomic distance and about 15% for the Debye−Waller factor.

Figure 11 shows the EXAFS spectra and FTs for the electrochemical extractions of Li^+ from the $Li_{3.07}CoO$ phase. The extraction of 0.75 mol of Li^+ from the $Li_{3.07}CoO$, $Li_{2.32}$-CoO phase shows that the FT peak intensities characteristic of the Co^0 phase decrease abruptly and weak FT peaks indicative of CoO evolve. The relative weakness of the FT peak features is due to the coexistence of the Co^0 and CoO phases in the Li_yCoO system.

Further extraction up to $Li_{1.51}CoO$ leads to a FT similar to the spectral feature of the pristine CoO, although the intensity of $Li_{1.51}CoO$ becomes weaker than that of the pristine CoO. Thus, the electrochemical insertion−extraction of about half of

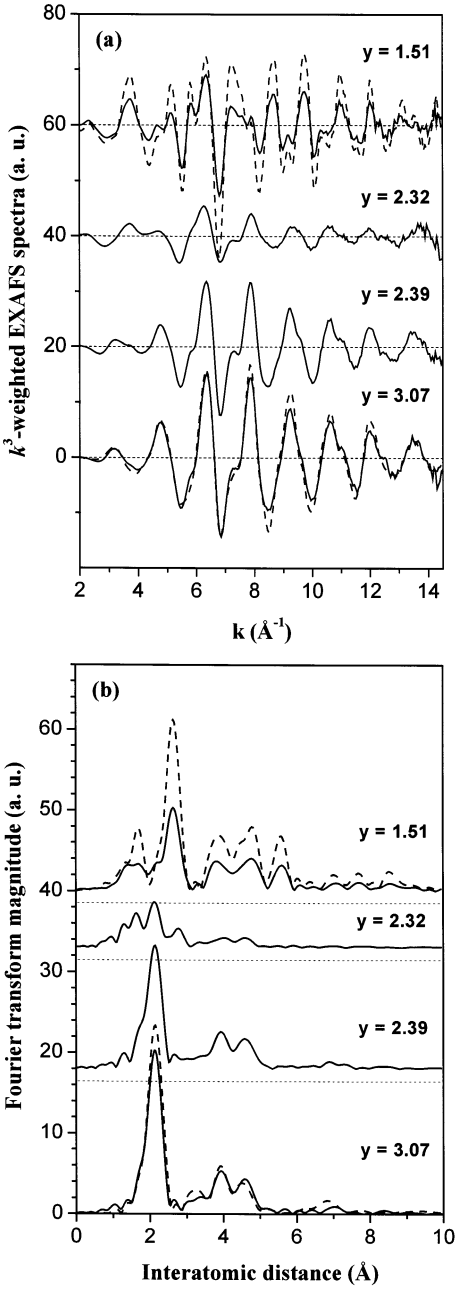

Figure 11. (a) Co K-edge $k^3\chi(k)$ spectra and (b) their Fourier transforms (FTs) for the electrochemically lithium-ion extracted Li_y-CoO system. The dashed lines in $y = 3.07$ and 1.51 indicate the EXAFS signals of the Co foil ($^2/_3$ amplitude) and CoO references, respectively.

the maximal lithium content (three lithium atoms per formula unit) at a current density of 0.5 mA/cm^2 is reversible for the first cycle. The reduced nanoscale Co^0 phase returns to the cubic CoO in the charging process. The FT features for the highest extraction of Li^+ are characteristic of the high-temperature cubic phase of CoO, in agreement with the XANES study. As mentioned above, the low-temperature phase with zinc blende type structure should show features different from those of the FT obtained for $Li_{1.51}CoO$. In the low-temperature phase, the cobalt ion is mainly located in a tetrahedral site, and corner-shared CoO_4 tetrahedral sites are distorted in the long range order. However, the present FT of the totally delithiated CoO does not show peak features corresponding to the low-temperature phase. In summary, the electrochemical reaction for the first cycle is reversible and the high-temperature cubic phase of CoO remains after the first cycle.

Conclusion

The local structures around Co atoms in cobalt oxide subjected to electrochemical insertion−extraction of Li^+ were investigated using Co K-edge X-ray absorption spectroscopy. The XANES and EXAFS spectra show marked variations over the first electrochemical cycle. The initial insertion of Li^+ leads to the reduction of the Co^{2+} in the pristine CoO to form the reduced metallic Co^0 state. The systematic variations observed in the peak intensities corresponding to the 1s → 3d and 1s → 4p transitions indicate that the mole ratio of Co to CoO increase gradually with the electrochemical insertion of Li^+ ions. The insertion of Li^+ causes the local structure around Co atoms to become asymmetric. The systematic decrease in FT magnitude with the increasing amount of inserted Li^+ is closely related to an increase in static disorder due to the presence of two phases: Co^0 and CoO. The small-sized Co particle evolves gradually with a well-separated distribution in the Li_2O matrix. In the successive extractions of Li^+, the reduced Co particles return reversibly to the high-temperature cubic phase of CoO.

Acknowledgment. The present study was supported by the Brain Korea 21 project. We are also grateful to the authorities in charge of the Pohang Light Source (PLS) for X-ray absorption spectroscopic measurements.

References and Notes

(1) Scrosati, B. *Electrochim. Acta* **2000**, *45*, 2461.
(2) Besenhard, J. O., Ed. *Handbook of Battery Materials*; VCH: Weinheim, 1998.
(3) Idota, Y.; Kubota, T.; Matsufuji, A.; Maekawa, Y.; Miyasaka, T. *Science* **1997**, *276*, 1395.
(4) Leroux, F.; Piffard, Y.; Ouvrard, G.; Mansot, J.-L.; Guyomard, D. *Chem. Mater.* **1999**, *11*, 2948.
(5) Denis, S.; Baudrin, E.; Touboul, M.; Tarascon, J.-M. *J. Electrochem. Soc.* **1997**, *144*, 4099.
(6) Courtney, I. A.; Dahn, J. R. *J. Electrochem. Soc.* **1997**, *144*, 2045.
(7) Courtney, I. A.; Dahn, J. R. *J. Electrochem. Soc.* **1997**, *144*, 2943.
(8) Poizot, P.; Laruelle, S.; Grugeon, S.; Dupont, L.; Tarascon, J.-M. *Nature* **2000**, *407*, 496.
(9) Grugeon, S.; Laruelle, S.; Herrera-Urbina, R.; Dupont, L.; Poizot, P.; Tarascon, J.-M. *J. Electrochem. Soc.* **2001**, *148*, A285.
(10) Obrovac, M. N.; Dunlap, R. A.; Sanderson, R. J.; Dahn, J. R. *J. Electrochem. Soc.* **2001**, *148*, A576.
(11) Westre, T. E.; Kennepohl, P.; DeWitt, J. G.; Hedman, B.; Hodgson, K. O.; Solomon, E. I. *J. Am. Chem. Soc.* **1997**, *119*, 6297.
(12) Shiro, Y.; Sato F.; Suzuki, T.; Iizuka, T.; Matsushita, T.; Oyanagi, H. *J. Am. Chem. Soc.* **1990**, *112*, 2921.
(13) Randall, C. R.; Shu, L.; Chiou, Y. M.; Hagen, K. S.; Ito, M.; Kitajima, N.; Lachicotte, R. J.; Zang, Y.; Que, L. *Inorg. Chem.* **1995**, *34*, 1036.
(14) Fronzoni, G.; Decleva, P.; Lisini, A. *Chem. Phys.* **1993**, *174*, 57.
(15) Rehr, J. J.; Leon, J. M.; Zabinsky, S. I.; Albers, R. C. *J. Am. Chem. Soc.* **1991**, 113, 5135.
(16) Kim, M. G.; Yo, C. H. *J. Phys. Chem. B* **1999**, *103*, 6457.
(17) O'Day, P. A.; Rehr, J. J.; Zabinsky, S. I.; Brown, G. E. *J. Am. Chem. Soc.* **1994**, *116*, 2938.
(18) Li, G. G.; Bridges, F.; Booth, C. H. *Phys. Rev. B* **1995**, *52*, 6332.
(19) Teo, B. K. *EXAFS: Basic Principles and Data Analysis*; Springer-Verlag: Berline, 1986.
(20) Koningsberger, D. C.; Prins, R. *X-ray Absorption: Principles, Applications, Techniques of EXAFS, SEXAFS and XANES*; Wiley-Interscience: New York, 1988.
(21) Ebbinghaus, S.; Fröba, M.; Reller, A. *J. Phys. Chem. B* **1997**, *101*, 9909.
(22) Zabinsky, S. I.; Rehr, J. J.; Ankudinov, A.; Albers, R. C.; Eller, M. J. *Phys. Rev. B* **1995**, *52*, 2995.
(23) Vaarkamp, M.; Dring, I.; Oldman, R. J.; Stern, E. A.; Koningsberger, D. C. *Phys. Rev. B* **1994**, *50*, 7872.
(24) Shin, H. J.; Chung, Y.; Kim, B. *J. Synchron. Radiat.* **1998,** *5*, 648.
(25) Yoon, W. S.; Kim, K. B.; Kim, M. G.; Lee, M. K.; Shin, H. J.; Lee, J. M.; Lee, J. S.; Yo, C. H. *J. Phys. Chem. B* **2002**, *106*, 2526.

(26) Kim, M. G.; Yo, C. H. *J. Phys. Chem. B* **1999**, *103*, 6457.
(27) Sekuliæ, A.; Furiæ, K.; Tonejc, A.; Tonejc, A. M.; Stubièar, M. *J. Mater. Sci. Lett.* **1997,** 16, 260.
(28) Almeida, E. C.; Abbate, M.; Rosolen, J. M. *Solid State Ionics* **2001**, *140*, 241.
(29) Warda, S. A.; Massa, W.; Reinen, D.; Hu, Z.; Kaindl, G.; de Groot, F. M. F. *J. Solid State Chem.* **1999**, *146*, 79.
(30) Montoro, L. A.; Abbate, M.; Rosolen, J. M. *J. Electrochem. Soc.* **2000**, *147*, 1651.
(31) Moodenbaugh, A. R.; Nielsen, B.; Sambasivan, S.; Fischer, D. A.; Friessnegg, T.; Aggarwal, S.; Ramesh, R.; Pfeffer, R. *Phys. Rev. B* **2000**, *61*, 5666.
(32) Park, J.-I.; Cheon, J. *J. Am. Chem. Soc.* **2001**, *123*, 5743.
(33) Herrero, E.; Li, J.; Abruna, H. D. *Electrochim. Acta* **1999**, *44*, 2385.
(34) Laruelle, S.; Poizot, P. Baudrin, E.; Briois, V.; Touboul, M.; Tarascon, J.-M. *J. Power Sources* **2001**, *97*−*98*, 251.
(35) Galoisy, L.; Cormier, L.; Clas, G.; Briois, V. *J. Non-Cryst. Solids* **2001**, *293*−*295*, 105.